

This is the accepted manuscript version of the contribution published as:

Budhraja, R., Karande, S., Ding, C., Ullrich, M.K., Wagner, S., Reemtsma, T., Adrian, L. (2021):

Characterization of membrane-bound metalloproteins in the anaerobic ammonium-oxidizing bacterium “*Candidatus* Kuenenia stuttgartiensis” strain CSTR1

Talanta **223, Part 2** , art. 121711

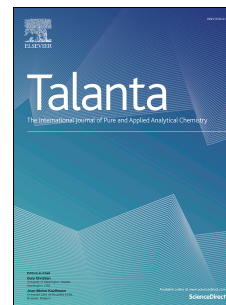
The publisher's version is available at:

<http://dx.doi.org/10.1016/j.talanta.2020.121711>

Journal Pre-proof

Characterization of membrane-bound metalloproteins in the anaerobic ammonium-oxidizing bacterium “*Candidatus Kuenenia stuttgartiensis*” strain CSTR1

Rohit Budhraj, Shubhangi Karande, Chang Ding, Maria K. Ullrich, Stephan Wagner, Thorsten Reemtsma, Lorenz Adrian



PII: S0039-9140(20)31002-X

DOI: <https://doi.org/10.1016/j.talanta.2020.121711>

Reference: TAL 121711

To appear in: *Talanta*

Received Date: 7 July 2020

Revised Date: 22 September 2020

Accepted Date: 25 September 2020

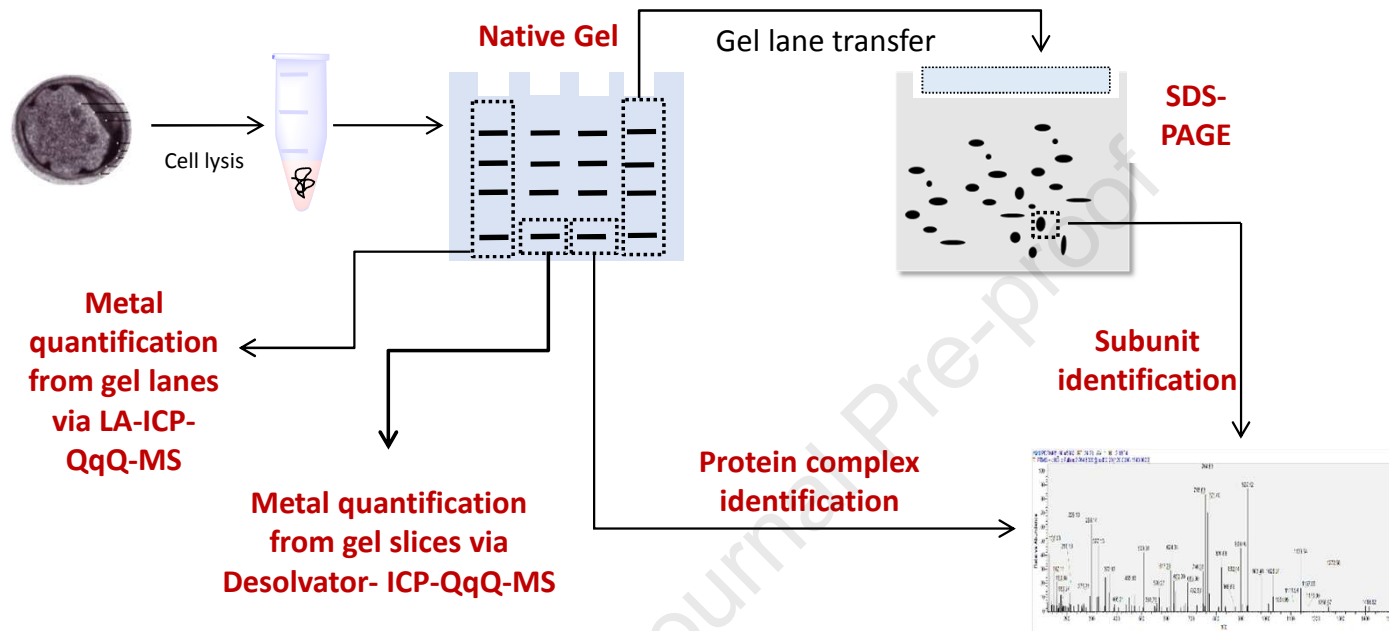
Please cite this article as: R. Budhraj, S. Karande, C. Ding, M.K. Ullrich, S. Wagner, T. Reemtsma, L. Adrian, Characterization of membrane-bound metalloproteins in the anaerobic ammonium-oxidizing bacterium “*Candidatus Kuenenia stuttgartiensis*” strain CSTR1, *Talanta*, <https://doi.org/10.1016/j.talanta.2020.121711>.

This is a PDF file of an article that has undergone enhancements after acceptance, such as the addition of a cover page and metadata, and formatting for readability, but it is not yet the definitive version of record. This version will undergo additional copyediting, typesetting and review before it is published in its final form, but we are providing this version to give early visibility of the article. Please note that, during the production process, errors may be discovered which could affect the content, and all legal disclaimers that apply to the journal pertain.

© 2020 Elsevier B.V. All rights reserved.

CRedit author statement

Rohit Budhreja: Conceptualization, Methodology, Investigation, Visualization, Writing- Original draft preparation. **Shubhangi Karande:** Methodology, Investigation. **Chang Ding:** Methodology, Resources, Writing- Reviewing and Editing. **Maria K. Ullrich:** Software, Writing- Reviewing and Editing. **Stephan Wagner:** Methodology, Software, Writing- Reviewing and Editing. **Thorsten Reemtsma:** Resources, Writing- Reviewing and Editing. **Lorenz Adrian:** Conceptualization, Resources, Visualization, Supervision, Project administration, Funding acquisition, Writing- Reviewing and Editing.



1 **Characterization of membrane-bound metalloproteins in the anaerobic**
2 **ammonium-oxidizing bacterium “*Candidatus Kuenenia stuttgartiensis*” strain**
3 **CSTR1**

4 Rohit Budhraj^{1,4}, Shubhangi Karande¹, Chang Ding³, Maria K. Ullrich², Stephan Wagner², Thorsten
5 Reemtsma², Lorenz Adrian^{3,4*}

6
7 ¹Helmholtz Centre for Environmental Research – UFZ, Isotope Biogeochemistry, Leipzig, Germany

8 ²Helmholtz Centre for Environmental Research – UFZ, Analytical Chemistry, Leipzig, Germany

9 ³Helmholtz Centre for Environmental Research – UFZ, Environmental Biotechnology, Leipzig, Germany

10 ⁴Chair of Geobiotechnology, Technische Universität Berlin, Berlin, Germany

11 *To whom correspondence should be addressed: Lorenz Adrian, Helmholtz Centre for Environmental
12 Research – UFZ, Environmental Biotechnology, Permoserstraße 15, 04318 Leipzig, Germany, Tel.: +49
13 341 235-1435, Fax: +49 341 235-1443, E-Mail: lorenz.adrian@ufz.de

14

15 Running title: *Kuenenia* metalloproteomics

16

17 Keywords: anammox; metallome; metalloproteomic; blue native gel electrophoresis; laser ablation;
18 desolvating nebulizer; ICP-MS

19

20 **Abstract**

21 Membrane-bound metalloproteins are the basis of biological energy conservation via respiratory
22 processes, however, their biochemical characterization is difficult. Here, we followed a gel-based
23 proteomics and metallomics approach to identify membrane-associated metalloproteins in the anaerobic
24 ammonium-oxidizing "*Candidatus* Kuenenia stuttgartiensis" strain CSTR1. Membrane-associated protein
25 complexes were separated by two dimensional Blue Native/SDS gel electrophoresis and subunits were
26 identified by mass spectrometry; protein-bound metal ions were quantified from the gel by connecting
27 either a desolvating nebulizer system or laser ablation to inductively coupled plasma triple quadrupole
28 mass spectrometry (ICP-QqQ-MS). We identified most protein complexes predicted to be involved in
29 anaerobic ammonium oxidation and carbon fixation. The ICP-QqQ-MS data showed the presence of Fe
30 and Zn in a wide range of high molecular weight protein complexes (230-800 kDa). Mo was prominently
31 found in gel slices with proteins of a size of 500-650 kDa, whereas Ni was only found using the
32 desolvating nebulizer system in the protein range of 350-500 kDa. The detected protein complexes and
33 their metal content were consistent with genome annotations. Gel-based metalloproteomics is a sensitive
34 and reliable approach for the characterization of metalloproteins and could be used to characterize many
35 multimeric metalloprotein complexes in biological systems.

36 **Introduction**

37 Metalloproteins are proteins to which a metal or a metal-containing cofactor is tightly bound. The bound
38 metals are often crucial for the biological activity of the protein [1]. About one-third of microbial proteins
39 contain metal ions and such metalloproteins have a significant role in many biological processes, e.g., in
40 the regulation of transcription and translation, respiration, photosynthesis, cell signaling, metal trafficking
41 and nitrogen fixation [2, 3]. Bacterial respiratory chains are formed by protein complexes, building an

42 electrically conductive path. Such conductive paths contain metals such as Fe, Ni, Co, Cu, Zn and Mo
43 among others [4, 5].

44 One biogeochemical system in which metalloproteins are of particularly high importance is the nitrogen
45 cycle. Intensive human activities, e.g. fertilizer application, have led to a surplus of nitrogen in the soil,
46 ground- and surface water and subsequently to eutrophication of surface waters, loss of biodiversity and
47 surface water acidification [6, 7]. Wastewater treatment plants play an important role in the removal of
48 nitrogen species from industrial, agricultural and municipal wastewater [8], however, nitrogen removal in
49 wastewater treatment plants consumes a lot of energy for nitrification and thereby contributes to climate
50 change. Anaerobic ammonium oxidation (anammox) is a microbially-mediated nitrogen removal process
51 requiring substantially less operating energy [9]. In this process, about half the ammonium in wastewater
52 is oxidized to nitrite and subsequently, ammonium and nitrite are combined in an exergonic reaction
53 sequence to dinitrogen [10]. The anammox process is catalyzed by anammox bacteria that were first
54 discovered in wastewater sludge in the early 1990s [11]. Yet, no pure strains are available and genomes
55 were determined using a metagenomics approach [12].

56 Using a semi-continuous stirred tank reactor we obtained a planktonic culture, enriched for about 90%
57 cells of "*Ca. Kuenenia stuttgartiensis*" strain CSTR1 [13] and recently determined the full genome of the
58 strain. The cytoplasm of anammox cells is divided into three compartments separated by bilayer
59 membranes [14]. The innermost compartment, the anammoxosome, occupies about 70-80% of the cell
60 volume and is surrounded by the anammoxosomal membrane [15]. The second compartment is the
61 riboplasm, and the third and outermost compartment the paryphoplasm [9]. Several important
62 biochemical studies have demonstrated that the anammoxosome is a dedicated compartment in which all
63 the catabolic reactions of the anammox metabolism take place, nitrogen is formed and energy is fixed [16,
64 17].

65 In these catabolic reactions, ammonium oxidation is linked to nitrite reduction, resulting in the formation
66 of nitric oxide and hydrazine as intermediates and nitrogen gas as final product. The electron flow

67 generated by these redox reactions is linked in a yet poorly-understood process to the generation of a
68 proton-motive force across the anammoxosome membrane and this proton-motive force is used as energy
69 source for ATP synthesis via ATPase. Key enzymes involved in the anammox process are nitrite
70 reductase, hydrazine synthase, hydrazine dehydrogenase, hydroxylamine oxidase and nitrite:nitrate
71 oxidoreductase (nitrate reductase) [16] all predicted to contain metals cofactors in their structure (Fig.
72 S1). However, nitrite reductase, which is predicted to be involved in the reduction of nitrite to nitric
73 oxide, was barely detectable in previous studies using mass spectrometric proteome analyses [16, 17].

74 We have recently studied whole cells of anammox and other bacteria for the presence of typical
75 respiration metals [18] showing that this methodology can document the growth mode and the genetic
76 composition of a strain. The analysis revealed the overall average metal content of cells under different
77 conditions but no information of the metal content of specific protein complexes. Therefore, we now
78 searched for a methodology with which the metal content of abundant proteins can be determined in
79 samples from intricate communities without the separation of individual protein complexes, an approach
80 that is known as '*metalloproteomics*' [2, 19].

81 For a metalloproteomics approach, it is necessary to separate protein complexes in their native state to
82 retain metals in the protein structure. This can be done for example by chromatography [20], field-flow
83 fractionation [21], density gradient centrifugation [22] or gel electrophoresis [23], yet, for every
84 separation method, there are several advantages and limitations [24].

85 Blue Native gel electrophoresis (BNE) has been shown to be a powerful and sensitive approach for the
86 separation of low quantity metalloprotein complexes without disturbing complex integrity [25, 26].
87 Protein complexes can then be excised from the gel and analyzed for protein and metal content, using LC-
88 MS/MS and ICP-MS, respectively. However, trace metal concentrations in combination with limited
89 sample volume present a major challenge for analysis. Performing analyses in dry plasma mode has been
90 shown to improve sensitivity for matrix-rich samples significantly [27, 28]. Also, a direct transfer of
91 metalloproteins from a gel to an inductively coupled plasma mass spectrometer (ICP-MS) was shown

92 using laser ablation (LA-ICP-MS), allowing imaging of metals in the gel and correlating metal with
93 protein abundance [29, 30].

94 Here we investigated strain CSTR1 for its membrane-bound metalloproteome by native extraction of
95 protein complexes from cells, separation of protein complexes by BNE and analysis of separated protein
96 complexes for metal and protein content. Proteins were analyzed by liquid chromatography mass
97 spectrometry (LC-MS/MS) and metals were analyzed by inductively coupled plasma triple quadrupole
98 mass spectrometry (ICP-QqQ-MS) employing triple quadrupole technology for the high-sensitivity
99 detection of Fe, Ni, Zn and Mo. In order to enhance detection capabilities further and simplify gel
100 preparation, two different modes of sample introduction were evaluated, using either a desolvating
101 nebulizer system to introduce excised and digested gel slices or coupling a laser to ICP-QqQ-MS for
102 direct ablation of the gel. The results give a comprehensive picture of metalloprotein complexes
103 expressed under the given cultivation conditions. Key enzymes of the anammox process were detected
104 and their metal cofactors were quantitatively analyzed.

105 **Experimental**

106 **Chemicals, bacterial strain and cultivation**

107 All chemicals used were at least of analytical quality and obtained from Merck or Sigma-Aldrich.
108 “*Candidatus* Kuenenia stuttgartiensis” strain CSTR1 was cultivated in a semi-continuous stirred tank
109 reactor under anoxic conditions, as previously described [13]. Under these conditions, cells grew
110 planktonic and strain CSTR1 was enriched to a population share of approximately 90% [13]. The culture
111 medium contained 60 mM ammonium as an electron donor, 60 mM nitrite as an electron acceptor, 1x
112 trace element solutions [18] and 10 mM of bicarbonate as pH buffer and carbon source for autotrophic
113 growth. No organic carbon source was added to the medium [13, 18]. The reactor was running

114 continuously at 3-d hydraulic retention time, and effluent was collected for metal and proteomics
115 analyses.

116 **Cell lysis and membrane isolation**

117 Cells were harvested from 100 mL of culture by centrifuging the culture at 6,000 g for 30 min at 25°C
118 (Type 5804 R, Eppendorf). Cell pellets were resuspended in 3 mL of 1x phosphate-buffered saline (PBS;
119 2.7 mM KCl, 137 mM NaCl, 1.8 mM KH₂PO₄, 10 mM Na₂HPO₄, pH 7.4). Cells were lysed by five
120 successive freeze/thaw cycles using liquid nitrogen for freezing and 45°C thawing temperature. Cell
121 debris was removed by centrifugation at 10,000 g for 10 min at 4°C. The supernatant containing soluble
122 and membrane proteins was further subjected to ultracentrifugation at 184,000 g for 1 h at 4°C (Optima
123 MAX-XP, Beckman Coulter). The pellet containing membrane proteins was solubilized in 1x PBS and
124 again subjected to ultracentrifugation at 184,000 g for 1 h at 4°C. The pellet was then solubilized in 1x
125 PBS containing 0.5% (w/v) n-dodecyl-β-D-maltoside (DDM) with incubation for 2 h on a thermomixer
126 (Thermomixer comfort, Eppendorf) with 700 rpm at 25°C. Proteins were quantified with the
127 bicinchoninic acid (BCA) assay (Thermo Scientific).

128 **Protein separation by two-dimensional BN/SDS-PAGE**

129 Membrane protein complexes were separated under native conditions by Blue Native gel electrophoresis
130 (BNE) using the Native PAGE Novex Bis-Tris gel system (Invitrogen). Pre-casted 4-16% linear
131 polyacrylamide gradient gels were used. 40 μg of membrane proteins in 18 μL of water were amended
132 with 0.6 μL of Invitrogen sample additive (containing coomassie blue G-250) and 6 μL of sample buffer,
133 and three replicates of this mixture were loaded onto gels. NativeMark unstained protein standard
134 (Invitrogen) was used as a molecular weight standard. Cathode and anode buffers were prepared
135 according to the manufacturer's manual. Gel electrophoresis was performed at room temperature and the
136 voltage was set to 150 V until the blue dye (coomassie blue) reached the end of the gel (approximately 90
137 min). After electrophoresis, the three replicate sample lanes and the molecular weight standard lane were

138 cut from the gel. The first sample lane and the molecular weight standard lane were stained with
139 coomassie blue R-250 to visualize protein distribution on the gel. Twelve bands on the sample lane were
140 excised and used for protein identification by LC-MS/MS analysis after trypsin digest (see below). The
141 sample well (molecular weight range of 1000-1250 kDa) was not further investigated (slice 13 in Fig.
142 S2A). The second sample lane was used for metal detection by ICP-QqQ-MS. The third sample lane was
143 used for a second-dimension separation by SDS-PAGE to separate the subunits in protein complexes. For
144 this second-dimension of a BN/SDS-PAGE the excised unstained sample lane from BNE was incubated
145 in 10 mL 'pre-treatment solution' (40 mM Tris-HCl, pH 6.8, 10 mg mL⁻¹ SDS, 30% (v/v) glycerol, 0.36 g
146 mL⁻¹ urea) amended with 5 mg mL⁻¹ dithiothreitol (DTT) for 10 min under gentle agitation. This gel lane
147 was then alkylated by incubating in 10 ml 'pre-treatment solution' amended with 45 mg mL⁻¹
148 iodoacetamide (IAA) for 10 min under gentle agitation. The treated lane was then placed horizontally on
149 the top of a self-casted 10% polyacrylamide gel containing 1 mg mL⁻¹ SDS. An adhesive tape
150 (Certoplast) with a thickness of 0.15 mm was pasted on the side of the 1.0 mm spacer plate and this plate
151 with a final thickness of 1.15 mm was used to cast the SDS gel. The SDS-PAGE gel was cast in a mini-
152 PROTEAN Bio-Rad casting apparatus. Gel electrophoresis was performed at room temperature and 100
153 V constant voltage until the bromophenol blue dye of the sample buffer reached the end of the gel (90-
154 120 min). The gel was then silver-stained [31].

155 **In-gel tryptic digestion of proteins**

156 After coomassie staining, the first replicate sample lane and the molecular weight standard lane from the
157 BNE gel were cut horizontally using razor blades into 12 gel slices for protein identification, each with
158 0.5 cm height. For the optimization of detergent concentration, the gel was cut into 13 slices also covering
159 the molecular weight range of 1000-1250 kDa to evaluate the effect of detergent concentration on protein
160 solubilization. In addition, 34 gel spots from silver-stained 2D-BN/SDS-PAGE gels (from the third
161 replicate sample lane) were excised. In a separate experiment for the optimization of detergent
162 concentration, gel lanes were cut into 13 slices also covering the molecular weight range of 1000-1250

163 kDa to evaluate the effect of detergent concentration on protein solubilization. Gel slices and gel spots
164 were first washed with double distilled water (ddH₂O) and then de-stained in a 1:1 (v/v) ratio of 100 mM
165 Na₂S₂O₃ and 30 mM K₃[Fe(CN)₆]. De-stained gel slices and spots were further dehydrated with 100%
166 acetonitrile and then rehydrated in 50 mM ammonium bicarbonate buffer. After rehydration, disulfide
167 bonds in proteins were reduced by incubating for 30 min in 10 mM DTT under gentle shaking and then
168 alkylated with 100 mM IAA for 30 min in the dark with gentle shaking. Proteins were digested with 0.1
169 µg of trypsin (proteomic sequencing grade, Promega) and incubated with gentle shaking overnight at
170 37°C. Tryptic peptides were extracted from gel pieces by incubating the gel piece twice in 200 µL
171 extraction buffer (50% acetonitrile, 5% formic acid) for 20 min at room temperature and merging the two
172 extracts. After extraction, peptides were lyophilized, resuspended in 10 µL of 0.1% formic acid, and
173 desalted using C₁₈ Zip Tip columns (Merck Millipore) before nLC-MS/MS analysis.

174 **LC-MS/MS analysis**

175 The desalted peptide mixture was dissolved in 15 µL 0.1% formic acid and then analyzed using an
176 Orbitrap Fusion Tribrid mass spectrometer (Thermo Scientific) equipped with a nanoLC system (Dionex
177 Ultimate 3000RSLC; Thermo Scientific). Peptides were separated at a flow rate of 0.3 µL min⁻¹ using a
178 linear gradient of 60 min by using eluent A (0.1% formic acid in water) and eluent B (80% (v/v)
179 acetonitrile, 0.1% formic acid in water) on an Acclaim Pep Map trap column (100 Å pore size, 5 µm
180 particle size, 0.3 × 5 mm, Thermo scientific). Peptides were ionized by a TriVersa NanoMate, Advion
181 electrospray ion source. The analysis was performed in positive mode using full MS scan analysis with an
182 MS¹ resolution of 120,000 in the Orbitrap mass analyzer [32]. The fragment ions (MS²) were scanned at a
183 resolution of 60,000.

184 Acquired MS/MS raw data after LC-MS/MS were analyzed using the software Proteome Discoverer
185 (v2.2, Thermo Fisher Scientific). MS/MS data were searched against the annotated complete genome of
186 “*Ca. Kuenenia stuttgartiensis*” strain CSTR1 (Genbank accession number CP049055) for the
187 identification of proteins using SequestHT as a search engine. Error tolerance for precursor ion mass and

188 fragment ion mass was set to 3 ppm and 0.5 Da, respectively. Two missed cleavage sites were allowed.
189 Oxidation of methionine residues was set as dynamic modification, while carbamidomethylation of
190 cysteine residues was set as a fixed modification. The false discovery rate was kept <1% using the
191 Percolator node for the analysis at both protein and peptide levels. Protein and peptide abundance values
192 were calculated by intensity-based label-free quantification using the Minora node implemented in
193 Proteome Discoverer.

194 **Digestion of gel slices for metal quantification**

195 The unstained, second gel lane from the BNE gel was horizontally cut into 12 gel slices, each of 0.5 cm
196 height using a metal-free ceramic knife that was cleaned after every single cut. In parallel, 1.5 mL
197 Eppendorf vials were cleaned from potential metal contaminations by incubating them with 2% Suprapur
198 nitric acid (Merck Millipore) for 1 h and rinsing with metal-free ultrapure water. Metal-free ultrapure
199 water was prepared by incubating ddH₂O (1000 mL) with 10 mg Chelex-100 sodium form (Sigma) for 1
200 h at room temperature with gentle shaking, followed by filtration using 30-50 µm Whatman filter paper
201 (GE Healthcare). The gel slices were then transferred into the Eppendorf vials and digested in the open
202 vials with 200 µL of a 1:1 mixture of concentrated suprapur nitric acid (65%) and suprapur hydrogen
203 peroxide (Merck Millipore, 37%) by incubating them in a thermomixer at 100°C for 2 h. After this
204 procedure, no gel material was visible anymore and the solution was diluted with metal-free ultrapure
205 water up to 3 mL to achieve a final concentration of around 2% of nitric acid.

206 **Metal quantification from dissolved gel slices using a desolvating nebulizer system coupled** 207 **to ICP-QqQ-MS**

208 Metal concentrations in the digested gel slices were analyzed by direct injection into an Aridus II
209 desolvating c-flow nebulizer system (Teledyne CETAC) or a standard pneumatic 1000 µL min⁻¹ nebulizer
210 coupled to a high resolution 8800 ICP-QqQ-MS (Agilent Technologies). Calibration standards were
211 prepared by serially diluting the multi-element standard solution Merck XVI in the matrix solution

212 (digested blank gel pieces in 2% nitric acid) to concentrations between 0 and 10 $\mu\text{g L}^{-1}$. Rhodium (Merck
213 Millipore) was used as an internal standard at a final concentration of 1 $\mu\text{g L}^{-1}$.
214 Samples as well as multi-element standards were analyzed for the target metal isotopes ^{56}Fe , ^{60}Ni , ^{64}Zn ,
215 ^{95}Mo and ^{103}Rh . Argon sweep gas was set to a flow rate of 2.7 L min^{-1} , and nitrogen gas flow was set to 3
216 mL min^{-1} in the desolvating c-flow nebulizer system. Hydrogen was used as a reaction gas at a flow rate
217 of 2.5 mL min^{-1} in an Octopole Reaction System (ORS³). The operational parameters for the ICP-QqQ-
218 MS were optimized in dry plasma mode for high sensitivity towards the target metals (Table S1).
219 Concentrations of the target metals were also determined in slices from blank gels (without protein
220 samples) and subtracted from sample gels (with protein) for background correction. Other metals were
221 not analyzed to keep the focus on the most abundant protein complexes expected in Kuenenia.

222 **Metal analysis using a laser ablation coupled to ICP-QqQ-MS**

223 Metal content in gels was also determined directly by coupling a laser ablation system to the ICP-QqQ-
224 MS. Instead of dissolving gel slices in nitric acid and hydrogen peroxide, the material was ablated via a
225 laser beam and the thereby formed aerosol transported into the ICP-QqQ-MS for metal detection. For
226 that, an unstained lane of a BNE gel (carefully cut with a clean metal-free ceramic knife) was placed on
227 top of a wet cellophane sheet. A second wetted cellophane sheet was placed on top of the gel avoiding to
228 trap any air bubbles. The sandwich cellophane sheet with the gel lane in between was then encased in a
229 pair of acrylic frames where the sandwich was secured with tightly bound clips on the edges of the acrylic
230 frames and dried overnight at 60°C. The dried gel was mounted on a microscopic slide with double-sided
231 tape and placed in the sample chamber (HELIX II, Teledyne) of the laser ablation system (Analyte G2,
232 Teledyne CETAC), which was coupled to the 8800 ICP-QqQ-MS. The laser system was operated at a
233 fixed wavelength of 193 nm with a scan speed of 156 $\mu\text{m s}^{-1}$ and a repetition rate of 2 Hz. Helium gas was
234 used with a flow rate of 0.8 L min^{-1} for aerosol transfer from the ablation chamber to the ICP-QqQ-MS.
235 This aerosol was then diluted with argon gas using a flow rate of 220 mL min^{-1} . The instrumental
236 parameters (Table S1) for laser and ICP-QqQ-MS were optimized towards maximum sensitivity.

237 **Results**

238 **Metal content in the membrane fraction of "*Ca. Kuenenia stuttgartiensis*" strain CSTR1**

239 Whole cells and the isolated membrane fraction of "*Ca. Kuenenia stuttgartiensis*" strain CSTR1 were
240 analyzed after digestion for Fe, Ni, Zn and Mo content using the direct infusion mode in ICP-QqQ-MS.
241 The absolute amount of Fe, Ni, Zn and Mo in whole-cells was determined to be 4.7×10^7 , 3.5×10^5 , $3.4 \times$
242 10^6 and 9.0×10^4 ions per cell, respectively. Of these amounts, 96% of Fe content (4.5×10^7 ions per
243 cell), 50% of Ni (1.7×10^5 ions per cell), 95% of Zn (3.2×10^6 ions per cell) and 64% of Mo (5.7×10^4
244 ions per cell) were located in the membrane fraction, respectively (Table S2).

245 **Effect of detergent concentration on membrane protein solubilization**

246 To obtain data indicating which proteins carry metals, we applied solubilized proteins from whole cells of
247 strain CSTR1 to our gel-based metalloproteome approach. Therefore, proteins were solubilized from
248 whole cells with four different DDM detergent concentrations 2%, 1%, 0.5% and 0.1% (w/v). Cell lysates
249 contained proteins from all three membranes (periplasmic, cytoplasmic and anammoxosome). Cell lysates
250 treated with different DDM concentrations were separated by BNE. After separation and before
251 Coomassie staining we observed a blue smear in the gel, that was at ~146 kDa for 2% DDM, ~120 kDa
252 for 1% DDM, ~100 kDa for 0.5% DDM and not visible for 0.1% DDM. This smear was visible also when
253 no protein was added indicating it came from the sample buffer dye. (Fig. S2A). After Coomassie
254 staining, additional strong bands were visible in all samples (Fig. S2A). Most prominent were three strong
255 bands between 242 and ~500 kDa, indicating the presence of very abundant multisubunit complexes in
256 the membrane proteome. Two distinct bands were visible at all DDM concentrations at around 720 kDa
257 and a fainter band at ~600 kDa for the three higher DDM concentrations. Below 240 kDa, no strong
258 consistent bands were observed (only the DDM concentration-dependent dye smear). All stained gel lanes
259 were then cut into 13 gel slices of the same height (0.5 cm) including the slice with the injection well and

260 subjected to in-gel digestion for protein identification by nLC-MS/MS. The proteomic analysis yielded a
261 total of 1540 unambiguously identified proteins for 2% DDM, 1586 for 1% DDM, 1695 for 0.5% DDM,
262 and 1462 for 0.1% DDM. This result revealed no notable difference in total protein identifications with
263 changing DDM concentration. For all DDM concentrations, the number of identified proteins was very
264 different in the different gel slices across the gel lane (Fig. S2B). The highest number of proteins was
265 identified in the slices corresponding to a molecular weight range of 15-230 kDa with a maximum
266 between 30 and 70 kDa, corresponding to the expected size for monomeric proteins. In contrast, the slices
267 8-10 (230-650 kDa) containing a large amount of protein as indicated by coomassie staining (Fig. S2A)
268 contained a much lower number of different proteins indicating that these slices were dominated by few
269 multimeric protein complexes.

270 The four major bands visible in the BNE gel contained the following proteins: the bands at around 290
271 and 350 kDa contained hydrazine dehydrogenase, cation-specific pore-forming outer membrane protein
272 (OMP) and S-layer protein; the strong band at around 540 kDa and fainter band at 560 kDa contained
273 hydrazine synthase and nitrite:nitrate oxidoreductase; the bands at around 780 and 840 kDa contained
274 nitrite:nitrate oxidoreductase, Cpn60 chaperonin GroEL, the large subunit of GroESL and S-layer protein.
275 The abundances of all identified proteins in different gel slices after BNE and gel spots after SDS-PAGE
276 are given in Table S5.

277 In the next step, we evaluated the integrity of large protein complexes under the four different DDM
278 concentrations. For this, we analyzed in detail the migration pattern of two enzyme complexes described
279 to be trimeric: nitrite:nitrate oxidoreductase and hydrazine synthase. Both are described to be involved in
280 anaerobic ammonium oxidation. In the presence of different DDM concentrations, there was no
281 significant difference observed in the migration of different subunits of nitrite:nitrate oxidoreductase and
282 hydrazine synthase (Fig. 1). Remarkably, the intensity of all the subunits in both protein complexes was
283 higher in the presence of a high concentration of DDM. Still, we selected a DDM concentration of 0.5%

284 (w/v) for further analyses, because all major bands were visible in BNE (Fig. S2A) and the interference
285 with the dye of the sample buffer was less than at higher DDM concentrations.

286 **Composition of protein complexes in "*Ca. Kuenenia stuttgartiensis*" strain CSTR1**

287 To identify subunits of larger protein complexes and to understand the composition of the protein
288 complexes involved in the anammox process, we used a 2D BN/SDS-PAGE approach to first separate
289 membrane-bound protein complexes in their native state by BNE and then to separate their subunits in
290 denaturing conditions (SDS-PAGE). Membrane solubilization was done for isolated membrane fractions
291 after ultracentrifugation in 0.5% DDM to recover proteins from periplasmic, cytoplasmic and
292 anammoxosome membranes. We obtained samples from one lane of a blue native gel which was cut into
293 12 gel slices, excluding the top gel slice (1000-1250 kDa) consisting of non-separated proteins, but also
294 from the 2D gel after SDS-PAGE from which we cut many spots. Proteins within gel slices (from BNE)
295 or gel spots (from BN/SDS-PAGE) were identified by nLC-MS/MS (Fig. 2). The distribution of
296 identified proteins from these gel slices and spots are given in table S3.

297 All three subunits of nitrite:nitrate oxidoreductase (NAR) were detected together in the molecular weight
298 range 230-1000 kDa with the highest intensity in the range of 500-650 kDa in the first dimension
299 separation. These protein subunits were further detected in the second dimension with the molecular
300 weight of 148 kDa for NAR subunit alpha, 148 kDa for NAR subunit beta and 35 kDa for NAR subunit
301 gamma. The molecular weight of NirS is reported as 66.3 kDa, and it migrated at low abundance in the
302 molecular weight region of 70-230 kDa in the first dimension. This protein was detected in the second
303 dimension in spot 21, which represents a molecular weight region of 58 kDa. However, a protein, namely,
304 cation-specific pore-forming outer membrane protein (KsCSTR_06200) with a molecular weight of 61
305 kDa was the most abundant protein in gel spot 21 and covered around 90% of total protein abundance,
306 whereas NirS covered only 0.01% of the total abundance in this spot. The complexation of NirS with
307 other proteins could not be explained due to its low abundance. The heterotrimeric hydrazine synthase
308 (HZS) has a total molecular weight of 168.8 kDa, and all subunits migrated together with the highest

309 intensity in the range of 350-650 kDa in the first dimension. In second dimensional electrophoresis, these
310 subunits Hzs subunit alpha, and Hzs subunit beta, Hzs subunit gamma, were separated at the experimental
311 molecular mass 88, 39 and 38 kDa, respectively. Hydrazine dehydrogenase (HDH) and hydroxylamine
312 oxidase (HOX) were separated in the range of 230-350 kDa after first dimension separation, which were
313 also detected in the gel spot number 5 and 10 for HDH and spot number 3 and 7 for HOX after second
314 dimension separation with the highest intensity (Fig. 3).

315 Along with the key protein complexes involved in the anammox process and carbon fixation, the genome
316 of strain CSTR1 also encodes other FeS-cluster containing protein complexes involved in respiration and
317 energy generation such as NAD(P)H:quinone oxidoreductases (Complex I), Na⁺-translocating NADH-
318 quinone reductase (NQR), Rieske-cytochrome *b* complexes, ATPase and Na⁺-translocating
319 ferredoxin:NAD⁺ oxidoreductase complex. These proteins were found to be expressed in strain CSTR1
320 and were identified after both first-and second-dimension protein separation (Table S4).

321 As concluded from genome analysis NADH:ubiquinone oxidoreductase contains 13 subunits (NuoC and
322 NuoD subunits are fused to one) and most of the subunits were identified after the first-dimension
323 separation in gel slices of different molecular weight. Subunits NuoB, E, G, H and membrane-bound
324 subunits NuoL, M and N were identified with the highest intensity in the molecular weight range of 500-
325 650 kDa, whereas subunits NuoF, C, D, membrane-bound subunit J at 650-800 kDa and subunit NuoI
326 was identified at 30-50 kDa range after BNE. The membrane subunits NuoA and NuoK could not be
327 detected in our proteome analysis. The highest intensity of Na⁺-NQR protein subunits NqrC, E and F
328 were detected in the range of 230-350 kDa and for subunits NqrA and B, the intensity was observed
329 highest in the range of 170-230 kDa. Strain CSTR1 encodes three putative Rieske/Cytochrome *b*
330 complexes (R/*b*-1, R/*b*-2 and R/*b*-3). We identified all of them after first and second dimension
331 separation, where two of them (R/*b*-1 and R/*b*-3) were detected in the range of 110-170 kDa with the
332 highest intensity and R/*b*-2 was identified in the range of 650-800 kDa. “*Ca. K. stuttgartiensis*” strain
333 CSTR1 contains genes encoding four different types of ATPase, and our data demonstrated the

334 expression of several subunits of these ATPase after first and second dimension separation (Table S4).
335 The protein subunits of Na⁺-translocating ferredoxin:NAD⁺ oxidoreductase complex (RnfABCDEG) were
336 also found to be expressed in strain CSTR1. However, all the subunits were found in different molecular
337 weight regions after the first-dimension separation, probably due to instability of the complex under BNE
338 conditions (Table S4).

339 **Metal detection from gel slices using a desolvating nebulizer system coupled to ICP-QqQ-** 340 **MS**

341 The target metals (Fe, Ni, Zn and Mo) necessary for the membrane-bound protein complexes involved in
342 the anammox process were analyzed in the digested gel slices each with 0.5 cm height by ICP-QqQ-MS.
343 Two different types of sample nebulization were evaluated with respect to detection performance for the
344 target metal isotopes ⁵⁶Fe, ⁶⁰Ni, ⁶⁴Zn and ⁹⁵Mo, employing either a standard pneumatic 1000 μL min⁻¹
345 nebulizer (wet plasma mode) or a desolvating 50 μL min⁻¹ c-flow nebulizer (dry plasma mode). A strictly
346 linear response ($R^2 \geq 0.99$) was obtained for target metals Ni, Zn and Mo in the concentration range from
347 10 ng L⁻¹ to 1 μg L⁻¹ (corresponding to a concentration of 0.17 to 17 nM for Ni, 0.16 to 16 nM for Zn and
348 0.11 to 11 nM for Mo) and from 10 ng L⁻¹ to 10 μg L⁻¹ for Fe (0.18 to 180 nM) using both types of
349 sample nebulization. However, sensitivity of all target metals was substantially higher for the desolvating
350 nebulizer system than for the standard nebulizer (Fig. S3). The instrumental detection limits for Ni, Zn
351 and Mo were found to be 0.11 nM, 0.16 nM and 0.03 nM, respectively, which was around ten times lower
352 than without desolvating nebulizer (0.98 nM for Ni, 1.97 nM for Zn and 0.26 nM for Mo). Although the
353 detection limit for Fe was not enhanced by the desolvating nebulizer (Table 1), the marked increase in
354 sensitivity indicates the expanded detection capabilities in dry plasma mode (Fig. S3). Additionally, the
355 smaller flow rate of the desolvating nebulizer of 50 μL min⁻¹ led to a five-fold decrease in the total sample
356 volume (~ 60 μL) that is required for reliable ICP-QqQ-MS analysis. After considering 100% extraction
357 efficiency in 60 μL sample volume, a minimum amount of 125 fmoles of Fe-, 6.6 fmoles of Ni-, 9.6

358 fmoles of Zn- and 1.8 fmoles of Mo- containing proteins needed to be present in a gel slice to be detected
359 by ICP-QqQ-MS.

360 Based on the superior analytical performance, the desolvating nebulizer was chosen for the subsequent
361 quantification of Fe, Ni, Zn and Mo in gel slices from BNE. Over the entire molecular weight range, Fe
362 showed by far the highest concentrations of all the investigated metals, while Mo exhibited the smallest
363 values. Both Fe and Zn were detected in a wide molecular weight range of 230-800 kDa. Concentration of
364 Ni was found highest in the gel slices with a molecular weight range of 110-170 kDa and 350-500 kDa.
365 Mo was mainly observed in the gel slices representative of proteins with a molecular size of 170-230 and
366 500-650 kDa (Fig. 4).

367 **Metal detection directly from a gel lane using laser ablation**

368 Another unstained gel lane after first dimension separation (BNE) of proteins was scanned for target
369 metals using LA-ICP-QqQ-MS. Blank gel lanes without applied protein were used as a negative control.
370 With the laser ablation approach we obtained three continuous traces of metal data for each gel lane. The
371 highest intensity of Fe was present at distinct bands with protein size ranges of ~250-700 kDa, whereas
372 Mo was present only in one broader band in the protein size range of ~550-700 kDa. The patterns of
373 metal content along the triplicate gel traces obtained from laser ablation for Fe and Mo were similar to the
374 results obtained from the measurement of digested gel slices with desolvating nebulizer system coupled to
375 ICP-QqQ-MS. The intensity of Zn was observed highest in a high molecular weight range of 250-700
376 kDa, however, data for Zn showed considerable variation between the three replicate gel traces S1, S2
377 and S3. The intensity of Ni obtained by LA-ICP-QqQ-MS for the sample gel trace could not be
378 differentiated from the blank gel, which exhibited comparatively high background levels. A very low and
379 evenly distributed response was observed in blank gel lanes (without proteins) throughout the gel for Fe,
380 Zn and Mo (Fig. 5).

381 Discussion

382 Several membrane-bound respiratory complexes are expressed at high level at a time in a given organism
383 and their interplay and overall contribution to energy and redox metabolism is not well understood. One
384 example is the anammox model organism “*Ca. Kuenenia stuttgartiensis*” that contains several membrane-
385 bound complexes, some of which are not integrated into current metabolic models. Instead of focusing on
386 one metalloprotein complex we used an approach that looks at all strongly expressed membrane-bound
387 metalloprotein complexes together combining gel-based proteomics with gel-based metal analysis. Only
388 this gave us information on both, the identity of protein complexes and their metal content.

389 We and others have previously shown that this can additionally be linked with enzyme activity tests from
390 the same native gels [33, 34]. Separation of metalloprotein complexes on native gels, however, is only
391 possible with low amounts of protein ($\leq 10 \mu\text{g}$) and all applied detection methods must be reproducible
392 and sensitive. Whereas sensitive protein identification from gels by nLC-MS/MS and sensitive metal
393 quantification from solutions by triple quadrupole mass spectrometry (ICP-QqQ-MS) is standard [32, 34],
394 metal analysis from gels is not [29, 30].

395 The main goal of our work was the establishment of a workflow that gives us evidence for the presence of
396 metals in specific respiratory complexes. Neither whole-cell metallomics nor shotgun proteomics can
397 provide such a dataset because metal data cannot be associated directly to bottom-up proteomics data. We
398 therefore employed BNE with which we fully separated native respiratory protein complexes from small
399 monomeric proteins and with which we separated the native respiratory complexes from each other,
400 however, at low resolution. BNE therefore strongly reduced the complexity of the protein mixtures in our
401 high-molecular weight slices of the gel. Secondly we here focused on strongly expressed respiratory
402 protein complexes that are typically among the 10-20 most abundant proteins in shotgun proteomics
403 analyses. This allowed us to follow a quantitative approach where we correlate the strongest expressed
404 protein complexes with the most abundant metals. We here tested this approach as a proof of concept with

405 a new strain of “*Ca. Kuenenia stuttgartiensis*” membrane protein complexes and essentially obtain the
406 results that we expected from the review of the literature for protein complexes in other strains of this
407 organism. We conclude that the quantitative analysis of BNE-separated protein complexes is possible and
408 that the approach should be applicable to many other research questions in anaerobic microbiology.

409 We evaluated two different methods to efficiently and reliably extract metals from gels and to introduce
410 the extracted metals into an ICP-QqQ-MS system: i) total digestion of the gel matrix and transfer via a
411 desolvating nebulizer system, and ii) directly after ablating metal ions from a gel matrix with a laser
412 beam. The analysis with the desolvating nebulizer system was reliable, associated with less instrumental
413 effort and provided quantitative data. Furthermore, comparison between dry and wet plasma modes
414 demonstrated a substantial improvement of detection limits when using the desolvating nebulizer.
415 However, analysis of the metals from digested gel slices required extra attention to provide full digestion
416 of the gel matrix. To avoid metal contamination, metal extraction had to be done with many gel slices
417 carefully taken from the native gel under metal-free conditions. When using the laser ablation system
418 sample preparation was less complicated and analysis of metal distribution along the dried gels was
419 possible at high spatial resolution. Potentially, the sensitivity of the laser ablation setup is higher because
420 all the ablated material is transferred to the sample line [35]. However, the laser ablation approach needs
421 more expensive instrumentation and the analysis time on the instrument is longer. The qualitative results
422 obtained by these two independent approaches were mostly similar and supported each other in our study.

423 Metal contaminations during sample preparation are a major challenge because even slight metal
424 contamination leads to overestimation of the metal content in proteins and to non-stoichiometric results in
425 the metal ratios of a protein complex. We minimized metal contamination by using metal-free ultrapure
426 water for all used solutions and intensive washing procedures for gels and solid materials.

427 The genome annotation of “*Ca. Kuenenia stuttgartiensis*” suggests the presence of several Fe, Ni, Zn and
428 Mo-containing metalloprotein complexes. While Fe is predicted in many heme enzymes involved in the
429 anammox process and carbon fixation, Ni is predicted to be indicative of carbon fixation enzymes, Zn is

430 demonstrated to be prevalent in hydrazine synthase and Mo is predicted to be involved in nitrite oxidation
431 to nitrate which in anammox organisms is described to deliver electrons for CO₂ fixation [17, 36]. When
432 looking at whole membrane extracts of strain CSTR1 we detected all these four metals indicating that a
433 major share of these enzymes was associated with the membrane. The iron content was about 10-fold
434 higher than the content of other detected metals, highlighting the important role of Fe-containing
435 cofactors in the anammox process. However, we cannot exclude the presence of Fe particles in the
436 cytoplasm co-isolated with the membrane fraction.

437 Protein and metal detection in Blue Native gels identified several intact membrane-attached
438 metalloprotein complexes including nitrite reductase, hydrazine synthase, hydrazine dehydrogenase,
439 nitrite:nitrate oxidoreductase, hydroxylamine oxidase, carbon monoxide dehydrogenase/acetyl-CoA
440 synthase complex, NAD(P)H:quinone oxidoreductases (Complex I), Na⁺-translocating NADH-quinone
441 reductase, Rieske/cytochrome *b*- type protein complexes, ATPase and Na⁺-translocating ferredoxin:NAD⁺
442 oxidoreductase complex. The anammox process is described to occur in the anammoxosome lumen and
443 the key enzymes involved in this process are therefore expected to be localized in the lumen of
444 anammoxosome [37]. However, these enzymes were reported to be attached to the membrane [16] and
445 also in our study they are prominently present in the membrane fraction. One explanation could be that
446 the abundance of these protein complexes is very high in the cell and that a part of it was co-separated
447 with the membrane. The other possible explanation is that these complexes are bound to proteins at the
448 surface of the anammoxosome membrane. Subsequently, we analyzed in detail: i) the major anammox
449 complexes NIR, HZS and HDH; ii) the complexes HOX and NAR, and iii) the carbon fixation complex
450 CODH/ACS. The major BNE gel bands in the high molecular weight range (242-600 kDa) contained
451 NAR, HZS, and HDH which covered all together 60-80% of the total abundance of all identified proteins
452 in these bands. The high abundances of these protein complexes involved in the anammox process were
453 also reported in a previous study [16].

454 All three major anammox protein complexes and their predicted metals were found in the membrane
455 extracts. Nitrite reductase (NIR), encoded by *nirS*, is a dimeric protein with each monomer containing a c-
456 type heme and a d₁-type heme [12, 38] and its low expression was found at transcriptional [12, 17] and
457 protein level [16]. In our study, nitrite reductase was also low expressed possibly due to a high turnover
458 rate. Metal analysis demonstrated the presence of low amounts of Fe in the gel slice with nitrite reductase,
459 however, no Fe was detected with the laser ablation approach. As hypothesized before, alternative
460 proteins could catalyze nitrate reduction, such as HAO-like proteins [16, 17, 36, 39]. The genome of
461 strain CSTR1 contains genes for several putative HAO-like proteins (KsCSTR_04770, KsCSTR_29630,
462 KsCSTR_35890, KsCSTR_36130, KsCSTR_36400, KsCSTR_40830 and KsCSTR_49490) and two of
463 them were highly expressed in our study (KsCSTR_29630 and KsCSTR_49490). This confirmed earlier
464 reports of the high expression of these two paralogs (*kustc4574* and *kuste0458* in strain KUST) [39].

465 The second step of the anammox process is described as the reduction of nitric oxide to hydrazine by
466 hydrazine synthase (HZS). HZS is a dimer of a heterotrimeric protein complex and requires four heme
467 molecules and one zinc ion to perform its catalytic function [12, 40]. In our study, components of the
468 HZS complex migrated in a very broad range of molecular weight (110-800 kDa), which was confirmed
469 with the presence of iron and zinc ions in the same region using the desolvating nebulizer system.
470 Analysis with LA-ICP-QqQ-MS detected Fe in this molecular weight region, but no reproducible data
471 was obtained for zinc ions.

472 The third and final described step in the anammox process is the oxidation of hydrazine to dinitrogen gas
473 catalyzed by hydrazine dehydrogenase (HDH) [9, 17]. HDH is a homotrimeric enzyme, which forms
474 octamer of trimers in solution and harbors 192 c-type heme moieties [41]. The data obtained in our
475 study for the molecular weight range of 230-350 kDa corresponds well with both, the abundance of the
476 protein and with abundance of Fe in this region.

477 Hydroxylamine oxidase (HOX) belongs to the family of HAO-like enzymes and converts hydroxylamine
478 to nitric oxide [17]. HOX is described to be a homotrimeric protein with a monomeric mass of 62.4 kDa

479 harboring 24 heme c molecules [42]. We detected HOX in a molecular weight range of 230-350 kDa and
480 the metal data is consistent with predictions and suggests the presence of Fe in the same region. To obtain
481 electrons for carbon fixation anammox organisms oxidize nitrite to nitrate via nitrite:nitrate
482 oxidoreductase (NAR) [37], a heterotrimeric iron-molybdoenzyme located in the anammoxosome with a
483 predicted total mass of 215 kDa. Our data demonstrates the presence of this enzyme at a range of 500-650
484 kDa indicating the formation of a dimer or trimer of the heterotrimeric protein complex or co-eluting with
485 other proteins. Both Fe and Mo values were high in the corresponding gel region, suggesting that these
486 bands were correlating with the presence of NAR subunits.

487 Carbon-monoxide dehydrogenase /acetyl-CoA synthase (ACS) is a Ni- and Fe-containing enzyme
488 complex, which is crucial for autotrophic growth. In our study, ACS was detected in a low molecular
489 weight region (50-170 kDa) and the other Ni- and Fe-containing enzyme, carbon-monoxide
490 dehydrogenase 1 (CODH1) was identified in the high molecular weight region (500-650 kDa). CODH1 is
491 a soluble enzyme and predicted to be localized in the cytoplasm; its presence in the membrane fraction in
492 our study needs to be further evaluated. The metal analysis with both desolvating nebulizer system and
493 laser ablation showed the presence of Fe in the region of 500-650 kDa, however, unexpectedly Fe was
494 barely detected in the region of ACS expression, which we cannot explain currently. Ni was observed in
495 these corresponding gel regions using a desolvating nebulizer system, suggesting the involvement of Ni
496 containing cofactors in ACS and CODH1.

497 In the future, metalloproteomics should be extended to quantify metal ratios in metalloprotein complexes
498 and could be used for many other studies of biological systems.

499 **Data accessibility**

500 The mass spectrometry proteomics data have been deposited to the ProteomeXchange Consortium via the
501 PRIDE partner repository with the dataset identifier PXD018609.

502 Author contributions

503 R.B., S.K. and L.A. conceived the study and designed the experiments in coordination with S.W. and
504 M.K.U. The lab experiments were performed by R.B. and S.K. R.B., C.D. and L.A. analyzed the data.
505 R.B. and L.A. wrote the manuscript, and C.D., M.K.U., S.W. and T.R. contributed to the interpretation of
506 the data and edited the manuscript.

507 Competing interests

508 The authors declare that they have no competing interests.

509 Acknowledgments

510 The authors acknowledge Dr. Jürgen Mattusch and Timothy Ronald Holbrook for analytical support,
511 Benjamin Scheer and Felicitas Ehme for technical support. This work was financially supported by the
512 German Research Council (DFG) within the Research Unit SPP1927. Protein mass spectrometry was
513 done at the Centre for Chemical Microscopy (ProVIS) at the Helmholtz Centre for Environmental
514 Research, which is supported by European regional development funds (EFRE—Europe Funds Saxony)
515 and the Helmholtz Association.

516 Literature

- 517 [1] P.L. Hagedoorn, Microbial metalloproteomics, *Proteomes* 3 (2015) 424-439.
518 [2] W. Maret, Metalloproteomics, metalloproteomes, and the annotation of metalloproteins, *Metallomics*
519 2 (2010) 117-125.
520 [3] Z. Ma, F.E. Jacobsen, D.P. Giedroc, Metal transporters and metal sensors: how coordination
521 chemistry controls bacterial metal homeostasis, *Chem. Rev.* 109 (2009) 4644-4681.
522 [4] M. Jormakka, S. Törnroth, B. Byrne, S. Iwata, Molecular basis of proton motive force generation:
523 structure of formate dehydrogenase-N, *Science* 295 (2002) 1863-1868.

- 524 [5] R.G. Efremov, R. Baradaran, L.A. Sazanov, The architecture of respiratory complex I, *Nature* 465
525 (2010) 441–445.
- 526 [6] A. Miclea, W.R. Van Der Star, R. Kleerebezem, H.L. Banciu, The anammox process and its
527 applications in wastewater treatment, *Studia UBB Biologia* (2009) 97-110.
- 528 [7] C.J. Stevens, P. Manning, L.J. Van den Berg, M.C. De Graaf, G.W. Wamelink, A.W. Boxman, A.
529 Bleeker, P. Vergeer, M. Arroniz-Crespo, J. Limpens, Ecosystem responses to reduced and oxidised
530 nitrogen inputs in European terrestrial habitats, *Env. Pollut.* 159 (2011) 665-676.
- 531 [8] M.S. Jetten, M. Schmid, I. Schmidt, M. Wubben, U. Van Dongen, W. Abma, O. Sliemers, N.P.
532 Revsbech, H.J. Beaumont, L. Ottosen, Improved nitrogen removal by application of new nitrogen-cycle
533 bacteria, *Rev. Environ. Sci. Biotechnol.* 1 (2002) 51-63.
- 534 [9] L. van Niftrik, W.J. Geerts, E.G. van Donselaar, B.M. Humbel, R.I. Webb, J.A. Fuerst, A.J. Verkleij,
535 M.S. Jetten, M. Strous, Linking ultrastructure and function in four genera of anaerobic ammonium-
536 oxidizing bacteria: cell plan, glycogen storage, and localization of cytochrome c proteins, *J. Bacteriol.*
537 190 (2008) 708-717.
- 538 [10] J.G. Kuenen, Anammox bacteria: from discovery to application, *Nat. Rev. Microbiol.* 6 (2008) 320–
539 326.
- 540 [11] A. Mulder, A.A. Van de Graaf, L. Robertson, J. Kuenen, Anaerobic ammonium oxidation discovered
541 in a denitrifying fluidized bed reactor, *FEMS Microbiol. Ecol.* 16 (1995) 177-183.
- 542 [12] M. Strous, E. Pelletier, S. Mangenot, T. Rattei, A. Lehner, M.W. Taylor, M. Horn, H. Daims, D.
543 Bartol-Mavel, P. Wincker, Deciphering the evolution and metabolism of an anammox bacterium from a
544 community genome, *Nature* 440 (2006) 790–794.
- 545 [13] C. Ding, F.O. Enyi, L. Adrian, Anaerobic ammonium oxidation (anammox) with planktonic cells in
546 a redox-stable semicontinuous stirred-tank reactor, *Environ. Sci. Technol.* 52 (2018) 5671-5681.
- 547 [14] L. van Niftrik, M.S. Jetten, Anaerobic ammonium-oxidizing bacteria: unique microorganisms with
548 exceptional properties, *Microbiol. Mol. Biol. Rev.* 76 (2012) 585-96.
- 549 [15] L.A. van Niftrik, J.A. Fuerst, J.S.S. Damsté, J.G. Kuenen, M.S. Jetten, M. Strous, The
550 anammoxosome: an intracytoplasmic compartment in anammox bacteria, *FEMS Microbiol. Lett.* 233
551 (2004) 7-13.
- 552 [16] N.M. de Almeida, H.J. Wessels, R.M. de Graaf, C. Ferousi, M.S. Jetten, J.T. Keltjens, B. Kartal,
553 Membrane-bound electron transport systems of an anammox bacterium: a complexome analysis,
554 *Biochimica et Biophysica Acta - Bioenergetics* 1857 (2016) 1694-1704.
- 555 [17] B. Kartal, W.J. Maalcke, N.M. de Almeida, I. Cirpus, J. Gloerich, W. Geerts, H.J.O. den Camp, H.R.
556 Harhangi, E.M. Janssen-Megens, K.-J. Francoijs, Molecular mechanism of anaerobic ammonium
557 oxidation, *Nature* 479 (2011) 127–130.
- 558 [18] R. Budhreja, C. Ding, P. Walter, S. Wagner, T. Reemtsma, R.G. Sawers, L. Adrian, The impact of
559 species, respiration type, growth phase and genetic inventory on absolute metal content of intact bacterial
560 cells, *Metallomics* 11 (2019) 925-935.
- 561 [19] E.A. Roberts, B. Sarkar, Metalloproteomics: focus on metabolic issues relating to metals, *Curr. Opin.*
562 *Clin. Nutri. Metabolic Care* 17 (2014) 425-430.
- 563 [20] X. Yan, B. He, D. Wang, L. Hu, L. Liu, C. Liao, G. Jiang, Two-dimensional (weak anion exchange
564 chromatography-gel electrophoresis) separations coupling to inductively coupled plasma mass
565 spectrometry strategy for analysis of metalloproteins, *Talanta* 184 (2018) 404-410.

- 566 [21] K. Loeschner, C.F. Harrington, J.-L. Kearney, D.J. Langton, E.H. Larsen, Feasibility of asymmetric
567 flow field-flow fractionation coupled to ICP-MS for the characterization of wear metal particles and
568 metalloproteins in biofluids from hip replacement patients, *Anal. Bioanal. Chem.* 407 (2015) 4541-4554.
- 569 [22] P. Danaie, B. Wittmer, M. Altmann, H. Trachsel, Isolation of a protein complex containing
570 translation initiation factor Prt1 from *Saccharomyces cerevisiae*, *J. Biol. Chem.* 270 (1995) 4288-4292.
- 571 [23] A.-M. Sevcenco, G.C. Krijger, M.W. Pinkse, P.D. Verhaert, W.R. Hagen, P.-L. Hagedoorn,
572 Development of a generic approach to native metalloproteomics: application to the quantitative
573 identification of soluble copper proteins in *Escherichia coli*, *J. Biol. Inorg. Chem.* 14 (2009) 631-640.
- 574 [24] J.P. Barnett, D.J. Scanlan, C.A. Blindauer, Protein fractionation and detection for metalloproteomics:
575 challenges and approaches, *Anal. Bioanal. Chem.* 402 (2012) 3311-3322.
- 576 [25] J. Dresler, J. Klimentova, J. Stulik, Bacterial protein complexes investigation using blue native
577 PAGE, *Microbiol. Res.* 166 (2011) 47-62.
- 578 [26] J. Dresler, J. Klimentova, J. Stulik, *Francisella tularensis* membrane complexome by blue
579 native/SDS-PAGE, *J. Proteomics* 75 (2011) 257-269.
- 580 [27] D. Cardinal, L.Y. Alleman, J. De Jong, K. Ziegler, L. André, Isotopic composition of silicon
581 measured by multicollector plasma source mass spectrometry in dry plasma mode, *J. Anal. Atom. Spec.*
582 18 (2003) 213-218.
- 583 [28] J. Karasinski, E. Bulska, M. Wojciechowski, L. Halicz, A.A. Krata, High precision direct analysis of
584 magnesium isotope ratio by ion chromatography/multicollector-ICPMS using wet and dry plasma
585 conditions, *Talanta* 165 (2017) 64-68.
- 586 [29] M.P. Sullivan, S.J. Morrow, D.C. Goldstone, C.G. Hartinger, Gel electrophoresis in combination
587 with laser ablation-inductively coupled plasma mass spectrometry to quantify the interaction of cisplatin
588 with human serum albumin, *Electrophoresis* (2019) 2329-2335.
- 589 [30] C.-N. Tsang, J. Bianga, H. Sun, J. Szpunar, R. Lobinski, Probing of bismuth antiulcer drug targets in
590 *H. pylori* by laser ablation-inductively coupled plasma mass spectrometry, *Metallomics* 4 (2012) 277-283.
- 591 [31] M.V. Nesterenko, M. Tilley, S.J. Upton, A simple modification of Blum's silver stain method allows
592 for 30 minute detection of proteins in polyacrylamide gels, *J. Biochem. Biophys. Method* 28 (1994) 239-
593 242.
- 594 [32] K. Seidel, J. Kühnert, L. Adrian, The complexome of *Dehalococcoides mccartyi* reveals its
595 organohalide respiration-complex is modular, *Front. Microbiol.* 9 (2018) 1130-1143.
- 596 [33] C. Pinske, M. Jaroschinsky, F. Sargent, G. Sawers, Zymographic differentiation of [NiFe]-
597 hydrogenases 1, 2 and 3 of *Escherichia coli* K-12, *BMC Microbiol.* 12 (2012) 134.
- 598 [34] A. Kublik, D. Deobald, S. Hartwig, C.L. Schiffmann, A. Andrades, M. von Bergen, R.G. Sawers, L.
599 Adrian, Identification of a multi-protein reductive dehalogenase complex in *Dehalococcoides mccartyi*
600 strain CBDB1 suggests a protein-dependent respiratory electron transport chain obviating quinone
601 involvement, *Environ. Microbiol.* 18 (2016) 3044-3056.
- 602 [35] G.d.S. Pessoa, C.A.L. Júnior, K.C. Madrid, M.A. Arruda, A quantitative approach for Cd, Cu, Fe and
603 Mn through laser ablation imaging for evaluating the translocation and accumulation of metals in
604 sunflower seeds, *Talanta* 167 (2017) 317-324.
- 605 [36] B. Kartal, J.T. Keltjens, Anammox biochemistry: a tale of heme c proteins, *Trends Biochem. Sci.* 41
606 (2016) 998-1011.

- 607 [37] N.M. de Almeida, S. Neumann, R.J. Mesman, C. Ferousi, J.T. Keltjens, M.S. Jetten, B. Kartal, L.
608 van Niftrik, Immunogold localization of key metabolic enzymes in the anammoxosome and on the tubule-
609 like structures of *Kuenenia stuttgartiensis*, *J. Bacteriol.* 197 (2015) 2432-2441.
- 610 [38] A. Jafferji, J.W. Allen, S.J. Ferguson, V. Fülöp, X-ray crystallographic study of cyanide binding
611 provides Insights into the structure-function relationship for cytochrome cd1 nitrite reductase from
612 *Paracoccus pantotrophus*, *J. Biol. Chem.* 275 (2000) 25089-25094.
- 613 [39] B. Kartal, N.M. de Almeida, W.J. Maalcke, H.J. Op den Camp, M.S. Jetten, J.T. Keltjens, How to
614 make a living from anaerobic ammonium oxidation, *FEMS Microbiol. Rev.* 37 (2013) 428-461.
- 615 [40] A. Dietl, C. Ferousi, W.J. Maalcke, A. Menzel, S. de Vries, J.T. Keltjens, M.S. Jetten, B. Kartal, T.R.
616 Barends, The inner workings of the hydrazine synthase multiprotein complex, *Nature* 527 (2015) 394-
617 397.
- 618 [41] W.J. Maalcke, J. Reimann, S. de Vries, J.N. Butt, A. Dietl, N. Kip, U. Mersdorf, T.R. Barends, M.S.
619 Jetten, J.T. Keltjens, Characterization of anammox hydrazine dehydrogenase, a key N₂-producing enzyme
620 in the global nitrogen cycle, *J. Biol. Chem.* 291 (2016) 17077-17092.
- 621 [42] P. Cedervall, A.B. Hooper, C.M. Wilmot, Structural studies of hydroxylamine oxidoreductase reveal
622 a unique heme cofactor and a previously unidentified interaction partner, *Biochemistry* 52 (2013) 6211-
623 6218.
624

625 **Figure captions**

626 Fig. 1. Protein migration profile of different protein complexes in different DDM concentrations. (A) The migration
627 pattern of three different subunits (blue, orange and grey columns) of nitrite:nitrate oxidoreductase (NarI, NarH and
628 NarG), and (B) the migration pattern of components of hydrazine synthase (HzsC, HzsA and HzsB). In all graphs,
629 the distribution of protein subunits is plotted over the molecular weight (mw) range.

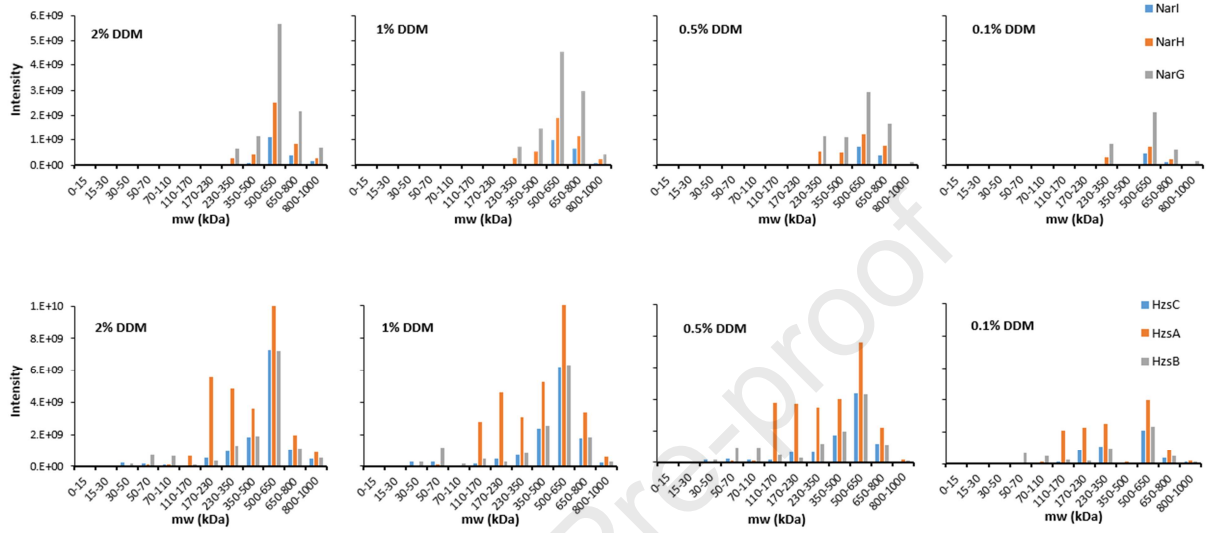
630 Fig. 2. Analysis of membrane-bound protein complexes of “Ca. Kuenenia stuttgartiensis” strain CSTR1 by 2D
631 BN/SDS-PAGE (A) Silver stained gel after first and second dimension separation. At the top of second dimension
632 gel (SDS-PAGE), a stained gel lane from the first dimension (BNE) is depicted together with a molecular mass scale
633 for BNE and on the left, a molecular mass scale for the second dimension (SDS-PAGE) is shown. In the actual
634 experiment a non-stained lane from BNE was transferred to the SDS-PAGE. (B) Schematic representation of gel
635 spots with the protein names identified by LC-MS/MS, which are annotated to be involved in the anammox process.
636 Subunits of the different protein complexes of strain CSTR1 are highlighted in colors (red: NIR, green: HZS,
637 yellow: HDH, blue: NAR, purple: HOX).

638 Fig. 3. Distribution of 0.5% DDM (w/v) solubilized protein complexes of “Ca. Kuenenia stuttgartiensis” strain
639 CSTR1 after first dimension (BNE) and second dimension (SDS-PAGE) separation. Left side graphs represent the
640 distribution with their intensities of nitrite:nitrate oxidoreductase (NAR) subunits (a), nitrite reductase (NirS) (b),
641 hydrazine synthase (HZS) subunits (c), hydrazine dehydrogenase (HDH) (d), hydroxylamine oxidase (HOX) (e) and
642 carbon monoxide dehydrogenase/acetyl-CoA synthase subunit alpha (ACS) (f) in different molecular weight ranges
643 of the BNE gel. Right side graphs represent the distribution and intensities of the single subunits in gel spots after
644 separation by SDS-PAGE.

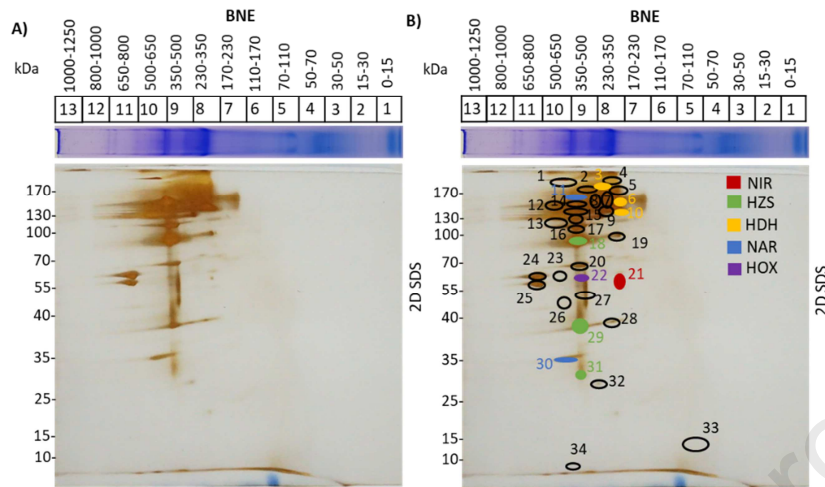
645 Fig. 4. Fe, Ni, Zn and Mo concentration determined by ICP-QqQ-MS coupled to a desolvating nebulizer system in
646 different slices of gel lanes loaded with 40 µg of strain CSTR1.

647 Fig. 5. False-color representation of metal analysis via LA-ICP-QqQ-MS of gel lanes loaded with 40 μg proteins of
648 strain CSTR1 (A, sample S1-S3) and blank gels (B, blank samples B1-B3) in three biological replicates. Intensities
649 obtained by the ICP-QqQ-MS are reported as counts per second (cps) below the samples (S1-S3) and blank gels
650 (B1-B3) for each element. A spot size of 156 μm and a laser moving speed of 156 $\mu\text{m s}^{-1}$ was used for ablation. The
651 molecular weight of the separated proteins is shown as a molecular mass scale on the left of every gel.

Journal Pre-proof

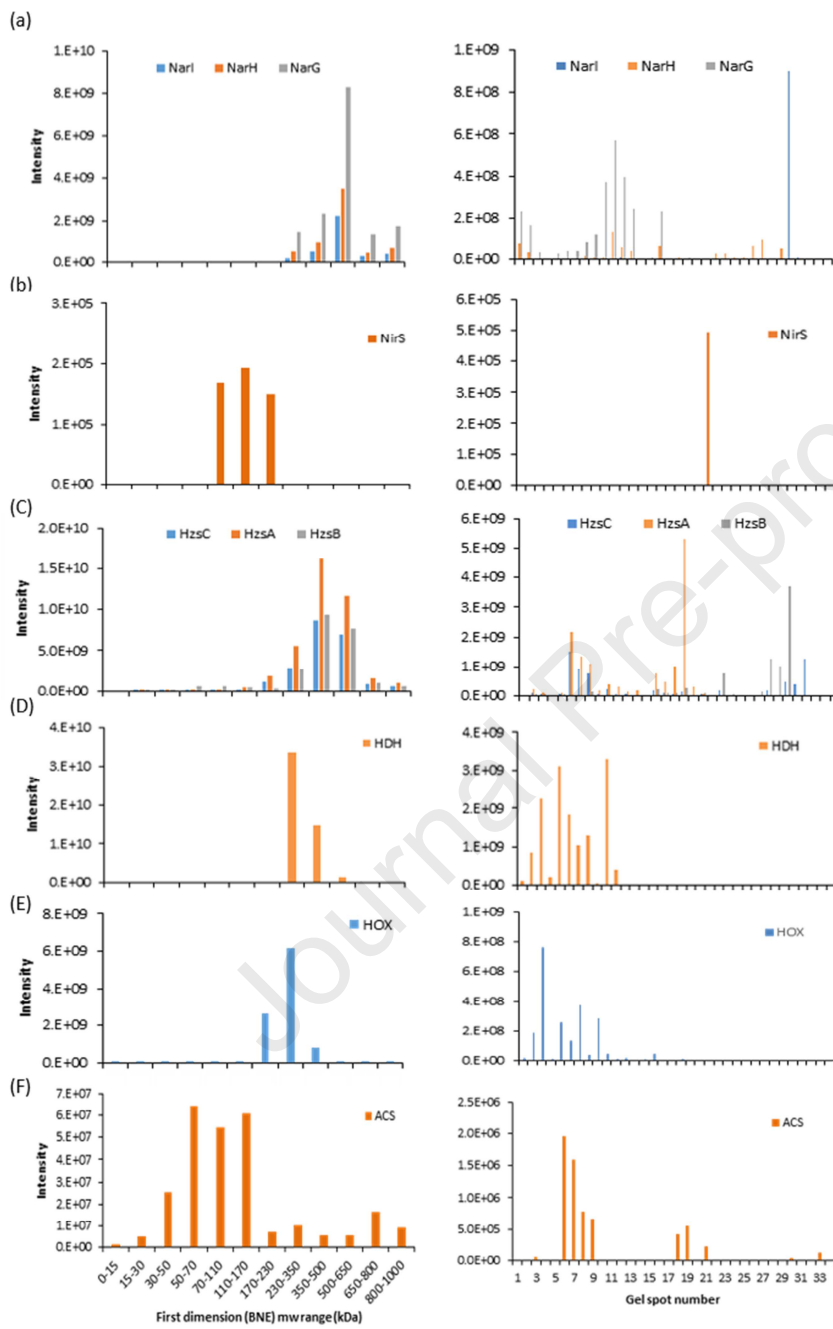
652 **Figures**653 **Fig. 1**

654

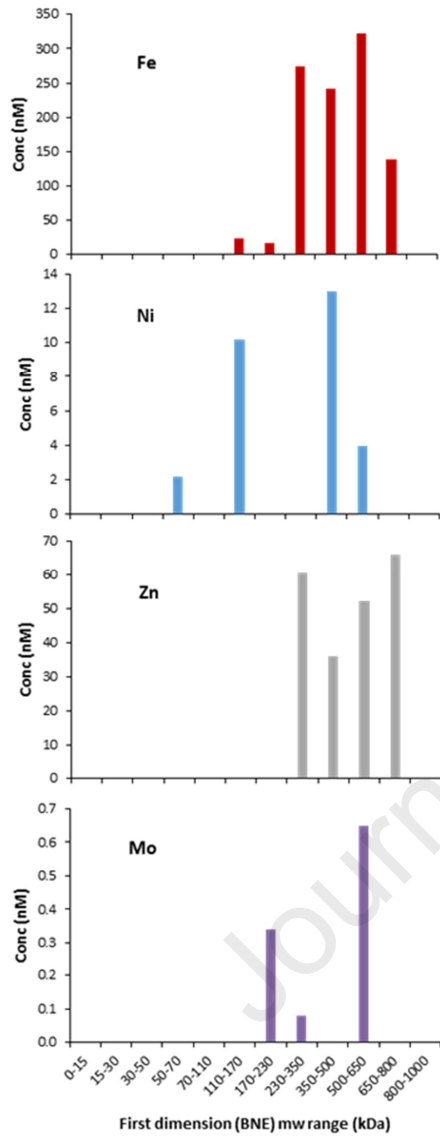
655 **Fig. 2**

656

657 Fig. 3

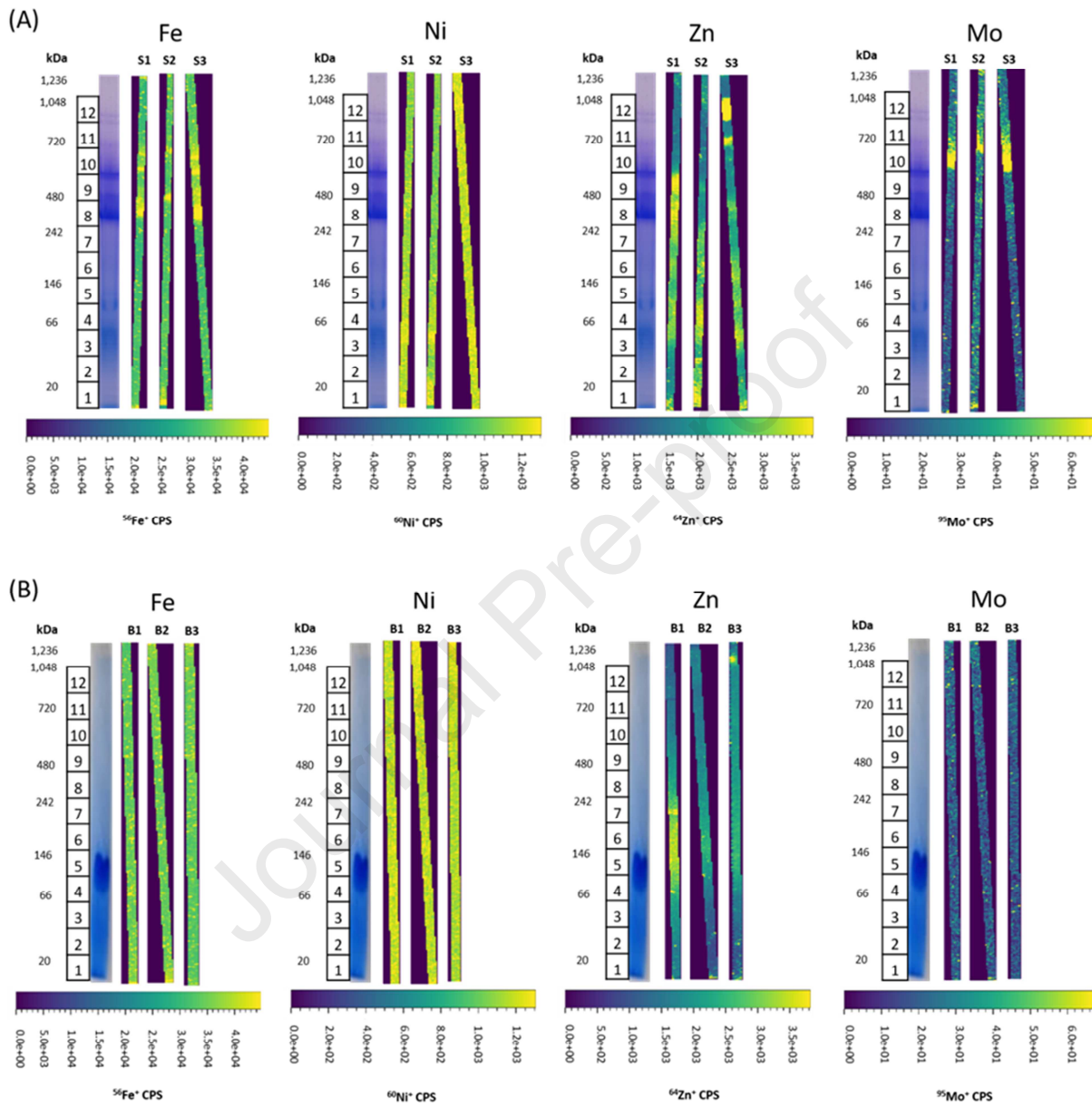


658

659 **Fig. 4**

660

661 Fig. 5



662

663 **Tables**

664 Table 1. The limit of detection (LOD) of ICP-QqQ-MS instrument with different nebulizer systems for different
665 metal isotopes.

Metal isotope	LOD (nM) with nebulizer (1000 $\mu\text{L min}^{-1}$)	LOD (nM) with desolvating c-flow nebulizer (50 $\mu\text{L min}^{-1}$)
^{56}Fe	2.68	2.08
^{60}Ni	0.98	0.11
^{64}Zn	1.97	0.16
^{95}Mo	0.26	0.03

666

Highlights

- Metalloproteins in anammox bacteria identified by gel-based metalloproteomics.
- 2D-BN/SDS PAGE to separate membrane-bound metalloprotein complexes.
- ICP-QqQ-MS sensitivity was improved with a desolvating nebulizer or laser ablation.
- Fe, Ni, Zn and Mo-containing abundantly expressed proteins were sensitively identified.

CRediT author statement

Rohit Budhraja: Conceptualization, Methodology, Investigation, Visualization, Writing- Original draft preparation. **Shubhangi Karande:** Methodology, Investigation. **Chang Ding:** Methodology, Resources, Writing- Reviewing and Editing. **Maria K. Ullrich:** Software, Writing- Reviewing and Editing. **Stephan Wagner:** Methodology, Software, Writing- Reviewing and Editing. **Thorsten Reemtsma:** Resources, Writing- Reviewing and Editing. **Lorenz Adrian:** Conceptualization, Resources, Visualization, Supervision, Project administration, Funding acquisition, Writing- Reviewing and Editing.

Declaration of interests

The authors declare that they have no known competing financial interests or personal relationships that could have appeared to influence the work reported in this paper.

The authors declare the following financial interests/personal relationships which may be considered as potential competing interests:

Journal Pre-proof